7.1 DROPSONDE DERIVED STRUCTURE OF MESOSCALE CONVECTIVE SYSTEMS OBSERVED DURING BAMEX

James Correia Jr and R. W. Arritt *, Dept. of Agronomy,
Iowa State University, Ames, IA

1. Introduction

The Bow echo And Mesoscale convective vortex EXperiment (BAMEX) utilized dropsondes to understand the thermodynamic variability within Mesoscale Convective Systems (MCS). Smull and Augustine (1993) documented the thermodynamic variability of a Mesoscale Convective Complex (MCC) during the PRE-STORM field campaign. They found significant thermodynamic variability across the asymmetric MCC including a cap in the suppressed convective region, deep layer saturation in the stratiform region, onion-type soundings (Zipser 1977) to the rear of the stratiform rain region, and *"subsaturated conditions ...and an ill-defined cloud base"*. Most soundings could not be launched in MCSs due to rain, lightning or icing which can lead to an early termination. Thus, we explore further the variability of the thermodynamics within MCSs with the unique dropsonde dataset.

2. Data and Methods

All 435 dropsonde profiles were examined subjectively for overall profile quality control (soundings were complete, absence of: a)significant sensor wetting, b)deep superadiabtic layers and horizontal winds were not erratic). The soundings were then classified based on structure of the low level thermodynamics. This gave us the opportunity to scrutinize the dataset before developing rigorous **spatial** criteria for classification.

2.1 *Sounding classification*

Soundings were classified based on the sonde horizontal position at the freezing level (GPS position when the temperature was 273K) and mapped onto the composite reflectivity from the surrounding WSR-88D. The soundings were then classified into 7 groups: environmental, leading line, transition region, stratiform rain region-main, stratiform rain region-center, stratiform region back-edge and wake. Table 1 lists dataset characteristics of the identified MCS subregions (shown schematically in figure 1).

* *Corresponding author address:* James Correia Jr., Iowa State University, Ames, IA 50010; e-mail: jimmyc@iastate.edu

2.2 *Sounding composite construction*

Sounding composites were constructed to preserve the low level thermodynamics by using the closest observation to the ground and freezing level as reference levels. The vertical coordinate then ranged from zero (presumed ground) to 1 (the freezing level) and higher (anvil layer). State variables that were composited include potential temperature, equivalent potential temperature, u,v, and retrieved w wind components. Each sounding used linear interpolation to conform to this vertical coordinate with a spacing of $\sim$35 m. Once each sounding was interpolated to the new coordinate, averages across the groups were performed to arrive at the composite vertical profile. Once the mean was determined we then calculated standard deviations of the variables.

2.3 *Vertical velocity retrieval*

In order to derive the vertical velocity we needed to remove the fall speed of the dropsonde. We acheived this by averaging all profiles according to an air density vertical coordinate. Density was chosen since the fall speed of the dropsonde is directly related to the air density. The sounding point values were then binned according to density. The binned data were averaged to arrive at a fall speed-density relationship and a sixth order polynomial was fit to the data (figure 2). Different bin widths yielded quantatively similiar results (not shown). The sixth order polynomial represents the average fall speed of the dropsonde. Quality control thresholds (any point value greater than 3 standard deviations above the mean) were applied and yielded very little change (less than 1% change at any level). The small change in dropsonde fall speed associated with quality control is evidence that the dropsonde fall speed is credible.

Next individual profiles of vertical velocity were examined to see how coherent the profiles were. We observed 38 profiles which were deemed corrupted (could not be fixed). The corrupt profiles were erratic (large level to level changes in vertical velocity) and had significant downward vertical velocity. These profiles were removed from the composite vertical velocity profiles.

We repeated the same procedure for the Rain In Cumulus over the Ocean experiment (RICO) dropsonde data as a reference (we also tried to use the IHOP data but it was corrupt for an unknown reason). The fallspeed of the dropsonde for the RICO and BAMEX datasets are nearly identical (figure 2).

Confidence intervals (90% ,figure 3) were computed as well at each density level and generally remain below 0.12 m s^{-1}. The confidence intervals for the RICO dataset were generally lower than 0.06 m s^{-1}. We believe that the difference between the RICO and BAMEX datasets is the result of BAMEX dropsondes being flown in active deep convection while RICO dropsondes were flown in shallow cumulus clouds with reduced variability of vertical velocity, weaker wind fields and thus weaker turbulent motions. Documented vertical velocities (e.g. see Knupp 1985 table 2.2) in strong precipitating downdraft cores (shallow) can vary between 1-10 m s^{-1}(0.5-6 m s^{-1}) while updrafts in strong convection can vary between 2-60 m s^{-1}(0.5-10m s^{-1}). We confirm that the standard deviation difference between the two datasets is 0.5-1 m s^{-1}(figure 4).

Our second attempt to verify that the signal we extracted was indeed the air vertical velocity used the environmental soundings (completely outside of deep moist convection). The mean vertical velocity profile for the environment was very close to zero (not shown) and the standard deviation was small. The small vertical velocity implies that we have extracted the air vertical velocity with an error of $\sim$ 0.1-0.2 m s^{-1}.

We then compared the relative frequency distributions of downdraft vertical velocity from the dropsondes (figure 5) with that obtained from the NOAA P3 aircraft during microphysical spirals (figure 6). The data are not taken at similiar spatio-temporal locations but are taken in the stratiform rain region exclusively. Thus we cannot relate a specific dropsonde to a specific spiral. Rather we use this data to check the magnitude and vertical location of the downdrafts sampled. The maximum frequency occurs at a vertical velocity of $\sim$0.5 m $s^{-1}$and extends from 1.25 to 6 km in both datasets. A relative frequency maxima appears near 4km between -3 and -2 m s^{-1}in both datasets. The 3% relative frequency contour occurs roughly near -2 m $s^{-1}$for both datasets. Thus it appears that the two datasets are very similiar which adds credibility to our retrieval technique.

3. Composite MCS

A composite cross section (figure 7) was constructed to elucidate the horizontal structure the soundings represent. The relative humidity field clearly shows that stratiform rain region and its rearward upward slope. Below the stratiform region the equivalent potential temperature is close to constant starting from the transition region (XWW) and extending rearward to the back edge of the reflectivity field (YWW). Curiously there is a second region where it is presumed the equivalent potential temperature field is constant along the rear edge of the reflectivity being deeper but weaker than the structure seen below the stratiform rain region.

Storm relative rear inflow extends along the gradient of the RH field but only until the stratiform rain region. Since the composite soundings were not constructed to preserve the rear inflow jet, it is encouraging that this feature is present. To arrive at the storm relative wind we used the average system motion of the leading line making no effort to incorporate local details (stratiform rain region movement, local cell propagation,etc). We leave this for future work.

The environment ahead of the MCS exhibits an elevated region of high relative humidity within the strong vertical gradient of equivalent potential temperature which ascends into the composite MCS. This structure is consistent with the finding that MCSs tend to be uncoupled from the surface layer and feed on a slightly elevated region of instability (Trier et al 2006).

The composite sounding of the stratiform rain region center and transition zone are shown in figures 8 and 9, respectively. The mean vertical velocity is downward from above the melting layer in the transition zone but downward from the melting layer in the stratiform rain region. The lack of a composite melting layer can be attributed to the shallowness of the melting layer in individual profiles, the presence of dry adiabatic layers across the 0°C isotherm, and

isothermal layers that occur between -2 to +3 °C . In some instances the lack of a melting layer potentially indicates that gradual sublimation, lack of significant melting or some other process may be at work. Storm and Parker (2006) identified a sounding during BAMEX in which sublimation accompanied by a downdraft may have caused the lack of isothermal layer near the melting level. Parker and Johnson (2004) noted that a similiar mechanism was identified in numerical simulations of leading stratiform MCSs.

4. Transition region

We define saturated profiles using the mean relative humidity between the surface and freezing level with saturated profiles having a mean RH of greater than 87%. We identified six saturated profiles in the transition region yet there were 28 unsaturated low level profiles. The unsaturated profiles are similiar to those documented previously in the transition zone (e.g. Schuur et al 1991, Marshall and Rust 1993, Shepherd et al 1996). It became apparent that proximity to the convective line, although important, was not the primary factor effecting the mean RH. As Braun and Houze (1994) point out it is the combination of microphysics (aggregation, size sorting, collection and growth of precipitation particles) and relative flow that determine the difference in radar reflectivity of the transition and stratiform rain regions. The significance of the saturated profiles is unknown but may be related to the evolution of the transition region.

Variability within the transition region (reflectivity minimum between the leading convective line and stratiform rain region reflectivity maxima) was confined to below the melting level for all soundings with slight variability above. Interesting structures seen are double dry layers in the lowest 150 hPa, dry adiabatic lapse rates extending toward the ground from the isothermal layer, a surface layer, and surface based stable layers. During the course of the analysis it became obvious that some of the structures could be attributed not only to the relative position but also to the evolution of the system. The evolutionary component was not accounted for due to the small sample size.

In general, the stratiform rain region and the transition region are very similiar. Both contain deep dry adiabtic lapse rates from the melting layer toward the ground and surface based stable layers. However, a number of soundings contained a double (low-level) inversion (figure 10 and 11). The lower inversion appears to be distinctly different thermodynamically (wet bulb potential temperature difference of 1-2K compared to the onion-type structure observed above). The thermodynamic characteristics of this low level inversion correspond to the properties of the low level inflow environment (either cooled from above or forced descent). Straka et al. (2006) and Wakimoto et al (2006) show that “up-down” downdrafts (Knupp et al 1987) were present in 3 case studies from BAMEX. The thermodynamic structure, observed in mutliple soundings from these particular case study days during or just after the time of their analysis, are consistent with “up-down” downdrafts.

Note how noisy the individual vertical velocity profiles can be. This is similiar to how the P3 aircraft vertical velocity data are noisy. Unfortunately due to random missing data a simple filter could not be designed and applied evenly across the data to preserve features greater than $2\delta z$. The profiles are coherent, however. In these two cases strong downdrafts were present in the deep dry adiabtic layer below the melting level. Notice how the moisture layers correspond to the vertical velocity. The 10 June case (figure 10) also contains a strong leading downdraft at the base of the elevated inversion potentially implying that the layer itself is sinking. Soundings taken later during this MCS show the two inversions eventually merge to produce a strong surface based inversion (not shown).

5. Results and future work

The results are summarized as follows.
1. The method used to retrieve vertical velocity was robust and could be confirmed with an independent dataset. Furthermore, vertical velocity retrieval from dropsondes aids in the interpretation of thermodynamic data.
2. The composite MCS agrees well with the conceptual model of MCSs. Thermodynamic variability was large in the transition and stratiform regions which included the presence of “saturated” low level soundings and shallow melting layers located between -2 and +3 °C .
3. Double low level inversions may be signatures of “up-down” downdrafts and were found primarily in the forward stratform rain and transition regions.

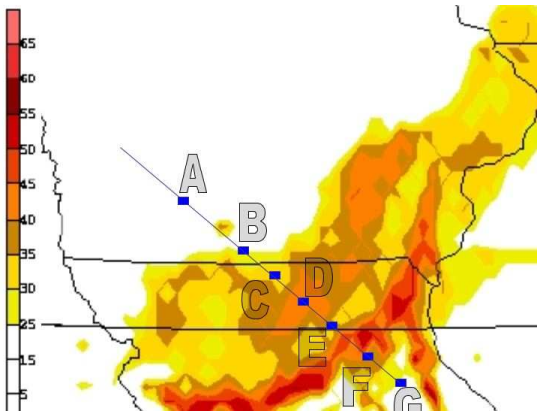

FIG. 1: Horizontal section of an example MCS and the areas used to place soundings in the composite with radar reflectivity is shaded. Regions are identified as follows: A. Wake, B. Stratiform-back edge, C. Stratiform-mid, D. Stratiform-Center, E. Transition, F. Leading Line, G. Environment.

Future work should include verifying high-resolution numerical weather prediction (NWP) models for physical processes with the dropsonde dataset. Low level structures are the result of both dynamical and microphysical processes and should be replicated by current NWP models. Perhaps new findings from NWP will shed light on other characteristics observed in the BAMEX dataset but not reported on here.

6. References

Available upon request.

MCS region	Total	Saturated	Mean dBz
Environment G	55	NA	NA
Leading Line F	34	NA	NA
Transition E	34	13	27
Strat. Center D	29	5	35
Strat. Grad C	43	8	25
Back edge B	11	2	15
Wake A	37	0	NA
Total	215	26	NA

Table 1: Table depicts the MCs subregion, number of soundings that fall into the classification, number of low level saturated soundings and the mean low level (course) reflectivity of the sonde at the freezing level.

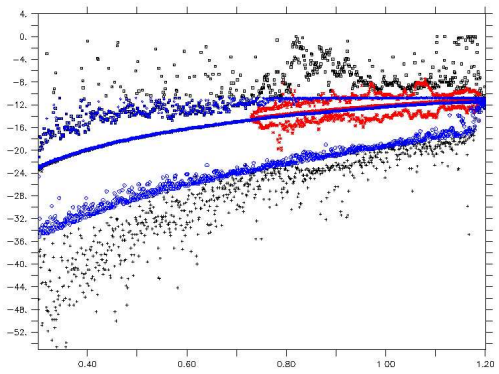

FIG. 2: Vertical velocity retrieval (solid), max and min value at each density level with (black) and without (blue) quality control. BAMEX (blue and black) and RICO (red) datasets are shown.

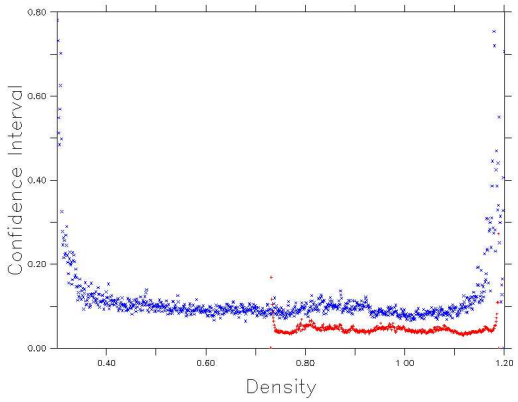

FIG. 3: Confidence interval for the BAMEX (blue) and RICO (red) datasets.

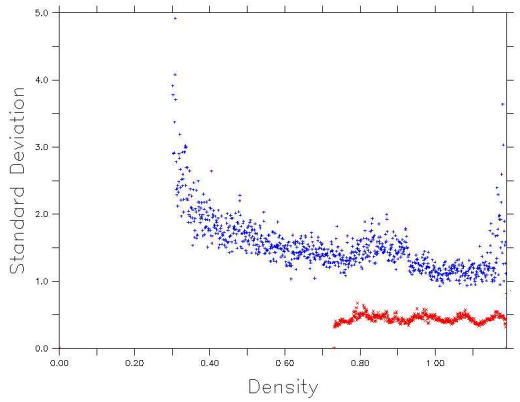

FIG. 4: Standard deviation of vertical velocity for BAMEX (blue) and RICO (red).

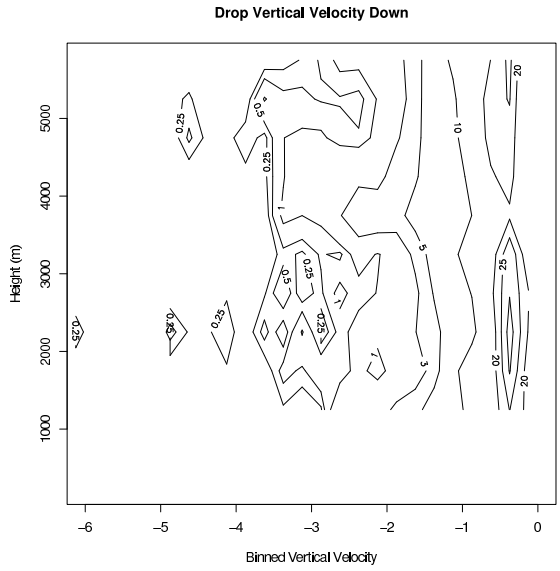

FIG. 5: Relative frequency distribution of downdrafts from the dropsonde binned in 500 m height increments and 0.25 m s^{-1}velocity increments.

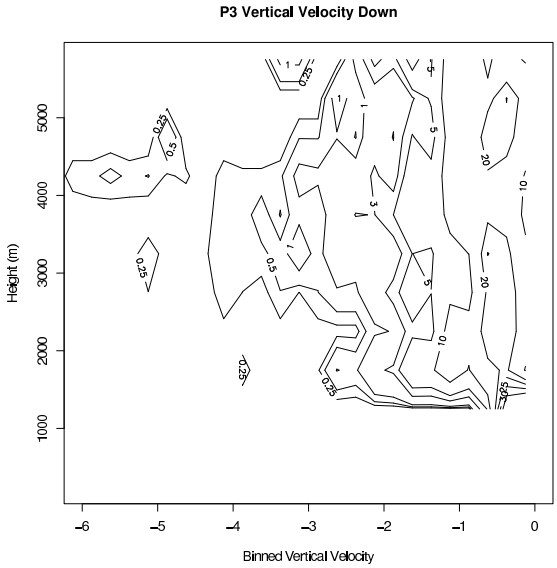

FIG. 6: Relative frequency distribution of downdrafts from the P3 during microphysical spirals binned in 500 m height increments and 0.25 m s^{-1}velocity increments.

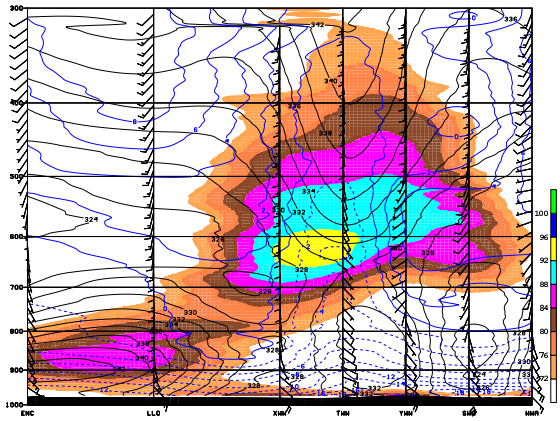

FIG. 7: Cross section of the composite vertical profiles with subregions G (left) to A (right). Relative humidity (shaded greater than 72%), equivalent potential temperature (contoured every 2 K) and relative u wind component.

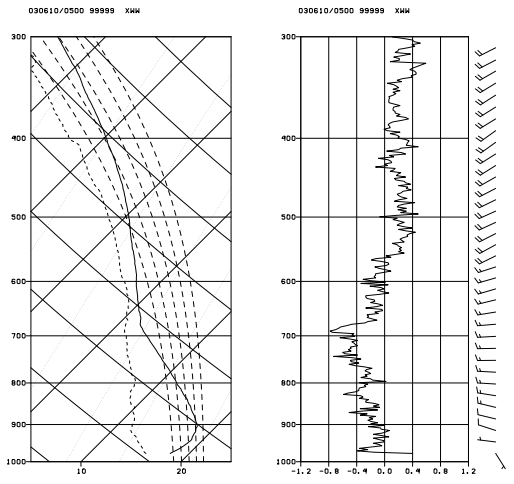

FIG. 8: Skew-T log p composite sounding in the transition zone.

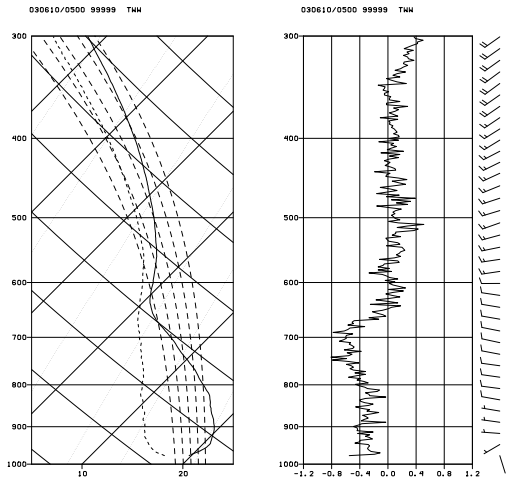

FIG. 9: Skew-T log p composite sounding in the Stratiform rain maximum zone.

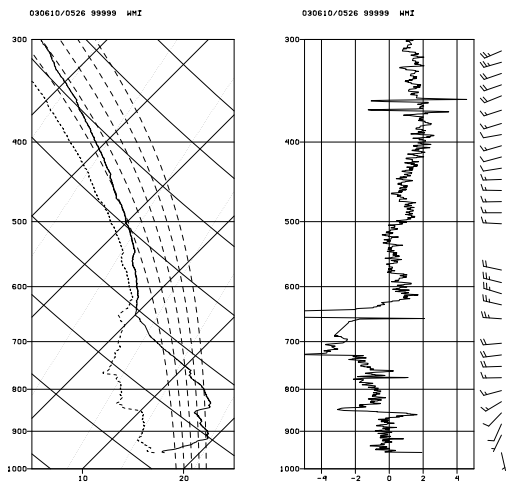

FIG. 10: Example of a double inversion from 10 June 2003 located in the transition region

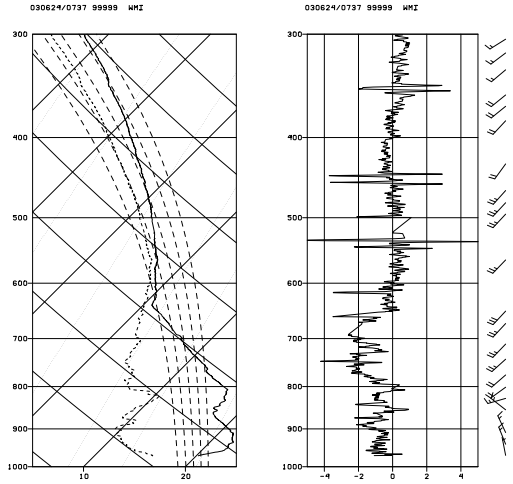

FIG. 11: Same as figure 10 except for 24 June 2003.